Aalborg Universitet

AALBORG UNIVERSITY
DENMARK

A Digital Signal Recovery Technique Using DNNs for LEO Satellite Communication Systems

Zhang, Yufeng; Wang, Zhugang ; Huang, Yonghui ; Wei, Wei; Pedersen, Gert Frølund; Shen, Ming

A Digital Signal Recovery Technique Using DNNs for LEO Satellite Communication Systems

Yufeng Zhang, Zhugang Wang, Yonghui Huang, Wei Wei, Gert Frølund Pedersen, *Senior Member, IEEE*, and Ming Shen, *Member, IEEE*

Abstract—This paper proposes a new digital signal recovery (DSR) technique for next-generation power efficient low Earth orbit (LEO) satellite-to-ground communication systems, which feature additive white Gaussian noise (AWGN) channel and significant power variation. This technique utilizes the prior knowledge (i.e., nonlinearities of radio frequency power amplifiers (RF-PAs)) of space-borne transmitters to improve the quality of the signal received at ground stations by modeling and mitigating the imperfection using deep neural networks (DNNs). Benefiting from its robustness against noise and power variation, the proposed DNN based DSR technique (DNN-DSR), can correct high signal distortions caused by the nonlinearities and hence allows RF-PAs to work close to their saturation region, leading to a high power efficiency of the LEO satellites. This work has been validated by both simulations and experiments, in comparison with the power back-off technique as well as memory polynomial based DSR solutions. Experimental results show that the DNN-DSR technique can increase the drain efficiency of the space-borne RF-PA from 32.6% to 45% while maintaining the same error vector magnitude as the power back-off technique. It has also been demonstrated that the proposed DNN-DSR technique can handle a signal power variation of 12 dB, which is challenging for conventional solutions.

Index Terms—deep learning, deep neural network, digital signal recovery, linearization, power amplifier, radio frequency, low Earth orbit, satellite-to-ground communication.

Fig. 1. System structure comparison between the linearization techniques. (a) Power back-off technique, (b) digital pre-distortion technique, (c) memory polynomial based digital signal recovery technique, (d) the proposed DNN based digital signal recovery technique.

I. INTRODUCTION

NOWADAYS, satellite communication has drawn great attention in the space industry due to the rapid technological advancement of low Earth orbit (LEO) satellites. LEO satellites are deployed at the altitude of 500–1500 km with an orbital period of shorter than two hours [1]. The fast movement of the LEO satellites leads to a very limited transmission

window with ground stations, approximately 10 minutes per pass. As the amount of data grows, transmitting as much data as possible is an increasing demand for LEO communication systems within the limited transmission window.

Orthogonal frequency division multiplexing (OFDM) techniques have been investigated for satellite communication to achieve a high transmission data rate [2]. However, the OFDM signal features a high peak-to-average power ratio (PAPR). This makes it very sensitive to system nonlinearities, which in most of the cases are mainly contributed by radio frequency power amplifiers (RF-PAs). Normally, the RF-PA works in saturated or near-saturated mode to achieve a high power efficiency, resulting in a high nonlinearity. The nonlinear distortion severely damages the signal quality (i.e., in-band distortion and out-of-band spectral regrowth), and hence degrades the transmission rate. Therefore, handling the nonlinearity of the RF-PA has been an indispensable part of LEO satellite-to-ground communication systems.

Power back-off techniques, which are illustrated in Fig. 1(a),
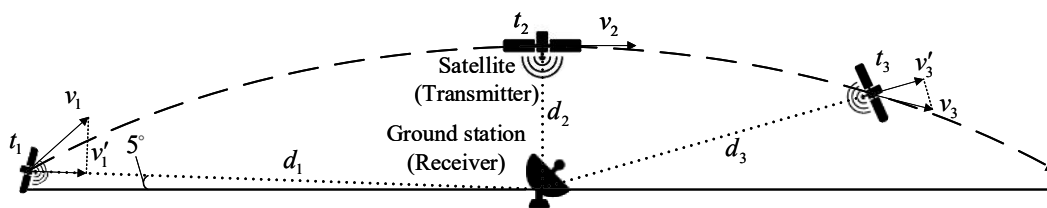
Fig. 2. Time-varying transmission distance of LEO satellite-to-ground communication systems.

are commonly used in LEO satellite-to-ground communication systems. The power back-off technique reduces the input power of the RF-PA to mitigate the nonlinear distortion of transmitted signals. Without consuming extra hardware resources and performing extra signal processing, space-borne transmitters become simple, reliable, and stable. However, the main drawback of the power back-off technique is the low power efficiency of the RF-PA. To improve the power efficiency of the RF-PA, different digital pre-distortion (DPD) techniques have been reported, such as lookup tables [3] and memory polynomial (MP) [4]. Also, deep neural networks (DNNs) based DPD techniques [5], [6] have been investigated due to their great linearization performance and attractive properties (e.g., robustness to dynamic nonlinearities of RF-PAs). As illustrated in Fig. 1(b) DPD techniques pre-distort the input of RF-PAs to compensate the nonlinearity, and as a result the output of the RF-PAs appears to be linearly amplified. DPD techniques could obtain both the superior signal quality and the high power efficiency. However, applying the DPD techniques into satellite communication is a great challenge due to the stringent limitation of power and computing resources available on satellites.

In this paper, we propose a new digital signal recovery (DSR) technique based on DNNs for next-generation power efficient LEO communication systems without using space-borne computing resources. The system block diagram is shown in Fig. 1(d). The novelty of this technique is the concept of capturing the nonlinearity of the space-borne RF-PA for recovering the received signal at the ground station. Very few work focusing on the DSR technique [7] has been reported previously. It is also possible to implement the proposed concept using the MP technique, as shown in Fig. 1(c). However, since the MP technique is power dependent, it only works under ideal channel conditions with a steady signal power. As illustrated in the results in the validation section, the MP-DSR technique does not work for satellite-to-ground communications which features time-varying channel effects, especially the time-varying signal power.

Driven by the more and more powerful computing resources and available data, DNNs have shown attractive potential in many different fields [8], [9]. Recently, a few DNN based techniques for boosting the performance of communication systems, such as autoencoders [10]–[12] have been reported. The proposed DNN-DSR concept is in line with this direction of the technology development. Benefiting from the robustness to noise provided by the DNN itself [8]–[10] and the power independence contributed by batch normalization layers, the proposed concept is becoming possible. This enables the
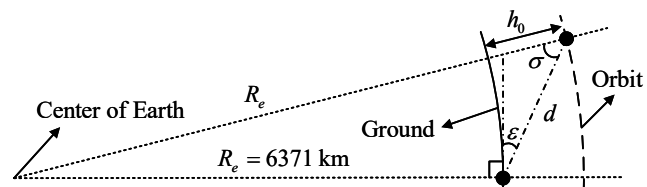
Fig. 3. Geometry change of the transmission distance.

space-borne RF-PA to work close to its saturation region, and hence achieves higher power efficiency.

The experimental validation compares the DNN-DSR technique with the power back off technique (Fig.1(a)) and the MP-DSR technique(Fig.1(c)). The comparison with the power back-off technique is with the focus on the drain efficiency of the space-borne RF-PA. And the comparison with the MP-DSR technique is focusing on the adjacent channel power rate (ACPR), AM-AM distortion, and error vector magnitude (EVM). The rest of this paper is organized as follows. Section II investigates the dynamic transmission condition. Section III shows the DNN theory, and section IV introduces the DNN-DSR technique. Validation of the proposed DNN-DSR technique is given in section V. Section VI presents the conclusion of this paper.

II. DYNAMIC TRANSMISSION CONDITION

A. Time-varying signal power

Generally, when the elevation angle of a LEO satellite is greater than $5°$, the transmission link is established [13], as shown in Fig. 2. At time t_1, the transmission link is set up with the longest transmission distance denoted as d_1. Meanwhile, the satellite is moving towards the ground station with a velocity of v'_1. At time t_2, the transmission distance is the shortest, and the relative velocity v'_2 is equal to zero. Finally, the satellite departs from the ground station with a relative velocity of v'_3.

The geometry relation between the elevation angle and the transmission distance can be built up in Fig. 3, where R_e represents the radius of Earth which is 6371 km, h_0 denotes the orbital altitude of the satellite, the elevation angle is represented as ε, and the transmission distance is denoted as d. Hence, the geometry relation between the elevation angle and the transmission distance is written as

$$\frac{R_e + h_0}{\sin\left(\frac{\pi}{2} + \varepsilon\right)} = \frac{R_e}{\sin \sigma} = \frac{d}{\sin\left(\frac{\pi}{2} - \varepsilon - \sigma\right)}. \quad (1)$$

Fig. 4. LEO transmission distance versus the elevation angle.
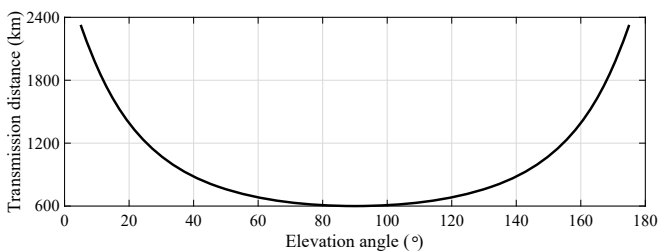

Fig. 5. Procedure of the DNN-DSR technique. (a) Offline training, (b) Online applying.

Referring to (1), the transmission distance d is obtained by

$$d = \frac{R_e + h_0}{\cos \varepsilon} \cdot \cos \left(\varepsilon + \sin^{-1} \left(\frac{R_e \cos \varepsilon}{R_e + h_0} \right) \right). \quad (2)$$

As an example, the transmission distance varying with the elevation angle, assuming a satellite orbit of 600 km, is shown in Fig. 4. On the other hand, the LEO satellite-to-ground transmission link is simply modeled as a point-to-point AWGN channel due to the negligible multi-path fading [13]. Hence, free-space path loss (FSPL) is the main contribution to the transmission loss in LEO satellite-to-ground communication. The FSPL is the attenuation of the radio energy, which depends on the signal wavelength and the transmission distance, and is defined as [13]

$$FSPL(\text{dB}) = 10 \log_{10} \left(\left(\frac{4\pi df}{c} \right)^2 \right)$$
$$= 20 \log_{10}(d) + 20 \log_{10}(f) - 147.56, \quad (3)$$

where f is the operating frequency in Hz, d is in m, and c is the light speed. When the orbital altitude of the satellite is 600 km, the longest transmission distance is 3.88 times longer than the shortest transmission distance. Therefore, the power of the received signal would have a variation of 11.8 dB.

Apart form the FSPL, there are also other factors, such as atmosphere absorption loss and antenna misalignment loss, which can also affect the received signal power. However, these effects are much smaller than the impact caused by time-varying FSPL, and therefore are not discussed in this paper.

B. Time-varying Doppler frequency

Because of the orbital motion, the Doppler frequency shift varies following an S-curve [14]. According to CCSDS standard 401.0-B-29 [15], the maximum rate of change of distance and velocity between the satellite and the ground station are 10 km/s and 380 m/s^2 respectively. Therefore, the Doppler frequency shift varies in the range of -270 kHz to 270 kHz with a maximum rate of change of 10 kHz/s for 8 GHz carrier frequency and -870 kHz to 870 kHz with a maximum rate of change of 34 kHz/s for 26 GHz carrier frequency.

The Doppler frequency shift can be compensated by both analog and digital methods [13], [16], [17]. In this paper, we assume an ideal compensation of the Doppler frequency shift before the DSR model.
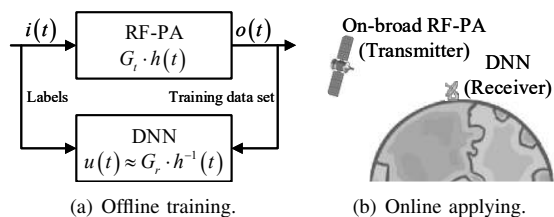
III. THE DNN THEORY

DNNs are composed of fully connected (FC) layers, batch normalization (BN) layers, and active function layers. Also, each hidden layer consists of one FC layer, one BN layer, and one active function layer.

In the FC layer, weights and biases are expressed by $\boldsymbol{W}_i$ and $\boldsymbol{B}_i$ respectively, where i denotes the i-th FC layer. Then, the output of the i-th FC layer $\boldsymbol{y}_i$ is defined as

$$\boldsymbol{y}_i = \boldsymbol{W}_i \boldsymbol{x}_i + \boldsymbol{B}_i, \quad (4)$$

where $\boldsymbol{x}_i$ is the input of the i-th FC layer. The number of neurons in each FC layer is determined by iterative tests to achieve the best performance.

Then, the output of the FC layer is sent into the BN layer. The BN layer normalizes the mean and variance of the input data to 0 and 1 respectively, and then gives the input data a new mean and variance. In this way, the time cost of the training step can be significantly reduced [18]. The output of the BN layer can be written as

$$\widehat{\boldsymbol{y}_i} = \boldsymbol{\gamma} \frac{\boldsymbol{y}_i - \mathrm{E}[\boldsymbol{y}_i]}{\sqrt{\mathrm{Var}[\boldsymbol{y}_i] + \epsilon}} + \boldsymbol{\beta}, \quad (5)$$

where $\widehat{\boldsymbol{y}_i}$ is the output of the BN layer. Also, $\boldsymbol{\gamma}$ and $\boldsymbol{\beta}$, which represent the new mean and variance of the input data, are the scaling and shifting parameters respectively. Note that, $\boldsymbol{\gamma}$ and $\boldsymbol{\beta}$ are learnable parameters. Besides, ϵ is a constant parameter that prevents the denominator from being zero. Generally, ϵ is set to 0.001.

Finally, the output of the BN layer is sent into the active function layer, which is expressed by $F(\cdot)$. $F(\cdot)$ is a nonlinear function such that the DNN becomes nonlinear. Owing to the nonlinearity, the DNN can fit arbitrary curves. The rectified linear units (ReLU) active function is used in the DNN-DSR technique for accelerating convergence [19]. The ReLU function is defined as

$$F_{ReLU}(u) = max(u, 0), \quad (6)$$

where u denotes the input of the ReLU function. Then, the output of one hidden layer can be expressed by

$$\boldsymbol{x}_{i+1} = max(\widehat{\boldsymbol{y}_i}, 0), \quad (7)$$

where x_{i+1} is the input of the next FC layer. This procedure that transfers the raw data from the first layer to the last layer is called the forward propagation. Useful features are extracted from the raw data layer by layer.
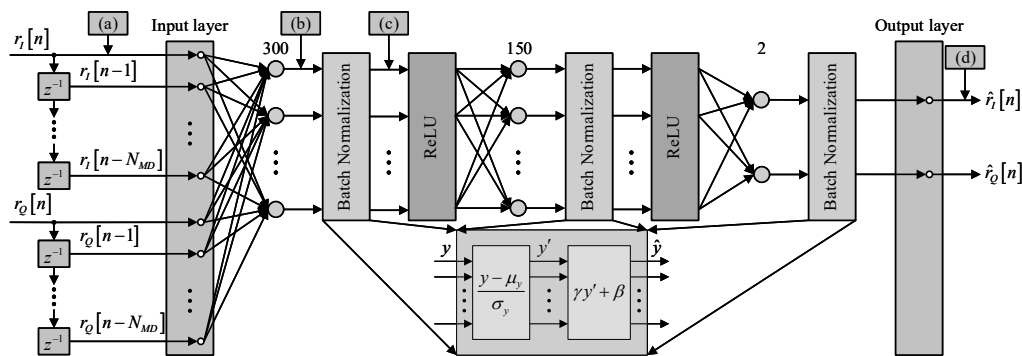
Fig. 6. Structure of the exploited DNN.

In this paper, the Smooth L1 loss function is utilized for regression due to its robustness to outliers [20]. Outliers represent the abnormal I/Q values that are extremely far from the true values in this work. The Smooth L1 loss function is represented by

$$Loss(O,T) = \frac{1}{N} \sum_{n=1}^{N} E_i, \tag{8}$$

where O and T are the predicted values and true values respectively, and

$$E_i = \begin{cases} 0.5 \left(O_i - T_i\right)^2, & \text{if } |O_i - T_i| < 1 \\ |O_i - T_i| - 0.5, & \text{otherwise} \end{cases}. \tag{9}$$

Besides, the adaptive moment estimation (Adam) algorithm is used for updating the weights of the DNN due to its computational efficiency [21]. The procedure that transfers the loss from the last layer to the first layer for updating the weights of the DNN is called backward propagation.

IV. PROPOSED DNN-DSR TECHNIQUE

A. Procedure of the DNN-DSR technique

The procedure of the DNN-DSR technique includes two steps (i.e., offline training and online applying), as shown in Fig. 5. In the offline training step, the DNN is trained to capture the nonlinearity of the RF-PA. The output and input of the RF-PA are set to the training data and true values, respectively, as shown in Fig. 5(a). Then, the DNN gradually learns the nonlinearity of the RF-PA during the training procedure. When the loss is under the preset threshold or no longer converged, the training step is finished. After training, the functionality of the DNN, denoted as $u(t)$, is an optimal estimation of $G_r \cdot h^{-1}(t)$, where $G_t \cdot G_r \approx 1$, and G_t is the gain of the RF-PA. In the online applying step, the trained DNN is placed at the ground station operating in the digital baseband. Meanwhile, the RF-PA that is learned by the DNN is assembled on the LEO satellite, as shown in Fig. 5(b).

Furthermore, considering extending the lifetime of satellites, the DNN-DSR technique needs to work with different or aging RF-PAs. In the first case, several backup RF-PAs will be assembled on the space-borne transmitter before the satellite is launched. Therefore, it provides enough time for the DNN-DSR technique to learn the nonlinearity of each RF-PA. In the

(a) Input of the DSR model.

(b) Input of the first batch normalization layer.

(c) Output of the first batch normalization layer.

(d) Output of the proposed DNN-DSR model.

(e) Output of the MP-DSR model.
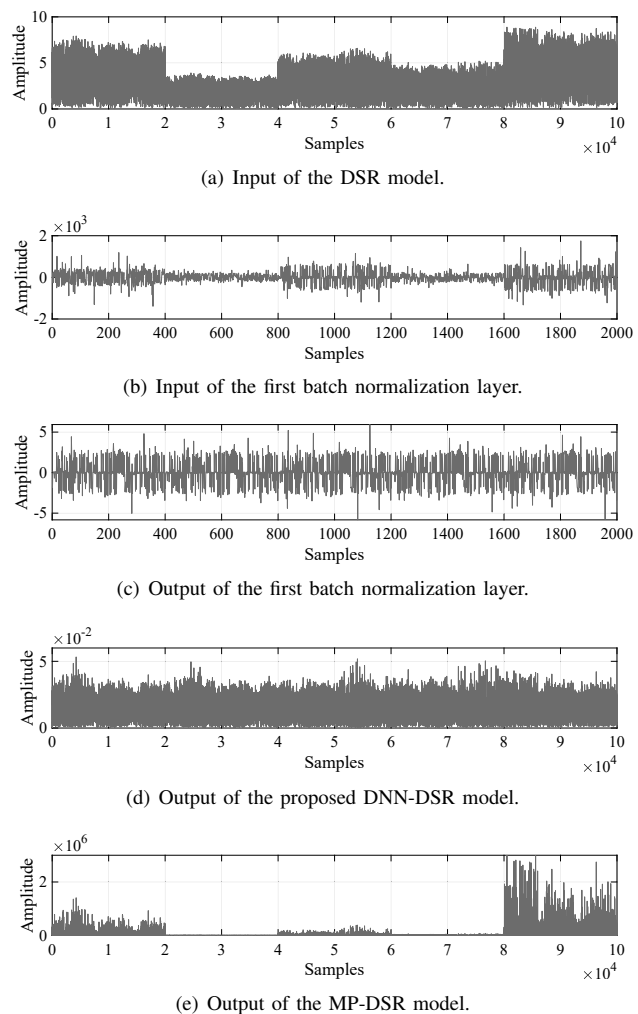
Fig. 7. Power variation of received signals. (a) Input of the two DSR models, (b) Input of the first batch normalization layer, (c) Output of the first batch normalization layer, (d) Output of the proposed DNN-DSR model, (e) Output of the MP-DSR model.

second case, the nonlinearity of the space-borne RF-PA varies with the temperature, voltage supply, and time. The DNN-DSR technique has the potential to update the DNN model online via transmitting training sequences from the satellite to the ground station without a feedback loop. However, online

updating of the DNN model is not the main focus of this paper, and it will be included in future work.

B. Principle analysis

The DSR technique typically encounters two critical challenges, which are the time-varying signal power and the AWGN. The DNN-DSR technique has two important features which well copes with these two challenges.

Firstly, the DNN-DSR technique is inherently robust to noise. In [8]–[10], DNNs appear robustness to noise if the training data are intentionally and randomly corrupted by noise. In other words, DNNs can learn the characteristics of the noise from the corrupted training data, and use the knowledge for improving the extraction of the data features. In this work, the captured output and input signals of RF-PAs are polluted by the thermal noise, which is a kind of AWGN. On the other hand, the principle of the MP-DSR technique is that different amplitudes of the output signal of the RF-PA are multiplied by different gains. Then, the output of the MP-DSR model appears to be linearly amplified. Therefore, the DNN-DSR technique appears more robust to the AWGN than the MP-DSR technique.

Another important feature of DNN-DSR is the power independence, which is achieved by including BN layers. The structure of the exploited DNN is shown in Fig. 6, where $r_I[n]$ and $r_Q[n]$ are Cartesian I/Q components of received signals. $\hat{r}_I[n]$ and $\hat{r}_Q[n]$ are the I/Q components of recovered signals. N_{MD} is the number of past samples that corresponds to the memory depth of MP techniques. (a), (b), (c), and (d) are the input of the DNN, the input of the first BN layer, the output of the first BN layer, and the output of DNN, respectively. The time-domain signals of (a), (b), (c), and (d) are shown in Fig. 7. It can be observed that the input power variation of the DNN has insignificant effect on the output of the DNN, and the first BN layer can keep the output power at a constant level. However, the MP-DSR model severely suffers from the time-varying signal power (Fig. 7(e)).

The mathematical model of the BN layer is shown in Fig. 6, corresponding to Eq. (5). The mean and the variance of the training data are both normalized by BN layers. In this paper, the mean and variance of the training data indicate the mean power and power variation of the input signal, respectively. Therefore, the BN layers can remove the characteristic of the time-varying signal power from the signal received at ground stations. Because of this advantage, the BN layer is inserted in every hidden layer, such that the time-varying signal power no longer affects the output of the DNN-DSR model. Therefore, the DNN-DSR technique is power independent by using the DNN with BN layers. However, referring to the principle of the MP-DSR technique, if the entire power level of the received signal changed, the MP coefficients would become completely incorrect. Therefore, the MP-DSR technique is a power dependent model and unsuited for the target application.

V. VALIDATION

A. Experimental setups

The radio frequency signal is generated by the signal generator and captured by the signal analyzer with MATLAB, as
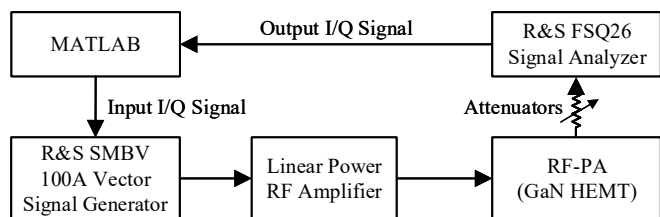
Fig. 8. Schematic diagram of the data collection system.
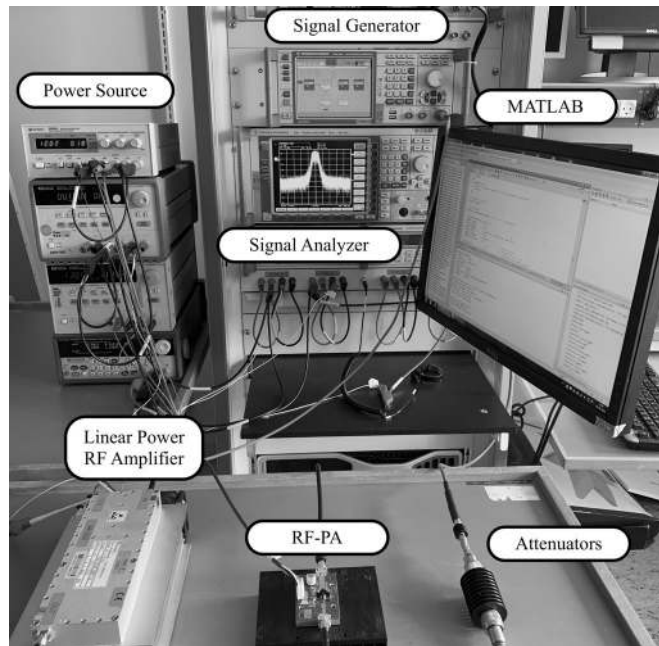
Fig. 9. Entire experimental environment.

shown in Fig. 8. The signal generator and the signal analyzer are R&S SMBV100A [22] and R&S FSQ26 [23] respectively. A CGH40006P RF-PA [24], which is a gallium nitride high electron mobility transistor, is used for testing the recovery performance. Furthermore, to have enough power to drive the RF-PA, the output of the signal generator is pre-amplified by a linear power RF amplifier [25]. The gain of the linear power RF amplifier can be approximately regarded as a constant number as the output power of the signal generator varies. The experimental environment is shown in Fig. 9.

In order to completely learn the nonlinearity of the RF-PA, the signal that is sensitive to the nonlinear distortion should be chosen in the experiments. In other words, it is necessary to find a signal with a high PAPR. In this experiment, we generate an OFDM signal with a PAPR of 10.06 dB directly from the signal generator. On the other hand, the frequency band and the carrier frequency of the signal are not the major concerns in this work. As C-band communication systems have already been deployed in satellites [26], the frequency band and the frequency point are set to 10 MHz and 3.5 GHz, respectively. Moreover, different input power levels of the RF-PA are taken into account for deriving the relation between the power efficiency of the RF-PA and the recovery performance, and different attenuators are inserted between the RF-PA and

TABLE I
RECOVERY PERFORMANCE VERSUS THE SIZE OF DNNs

Number of hidden layers and neurons	EVM[1]	ACPR[1,2]
1-10	2.55%	-40.19 dBc
1-100	2.38%	-40.65 dBc
1-300	1.83%	-43.01 dBc
1-500	1.59%	-43.91 dBc
1-10, 2-10	2.16%	-41.82 dBc
1-50, 2-50	1.51%	-44.63 dBc
1-100, 2-100	1.37%	-45.95 dBc
1-300, 2-150	1.33%	-46.74 dBc
1-500, 2-500	1.27%	-46.73 dBc

[1] The EVM and ACPR of the output signal of the RF-PA without DSR techniques are 8.06% and -32.06 dBc respectively.
[2] The ACPR of the input signal of the RF-PA is -50.03 dBc.

TABLE II
MODULATION FORMAT-DEPENDENT FACTOR

Modulation	PSK	16QAM	32QAM	64QAM
k^2	1	9/5	17/10	7/3

the signal analyzer to simulate the varying signal power.

On the other hand, the number of neurons and layers should be set appropriately. If the number of hidden layers and neurons is too small, the DNN cannot extract sufficient features from training data for linearizing the RF-PA (i.e., underfitting). In contrast, if the number of hidden layers and neurons is too large, the DNN will fit training data too closely (i.e., overfitting) and time will be wasted on training without any performance improvement or even have the risk of poor application performance. After testing the recovery performance versus different numbers of the neurons and layers, two hidden layers employed with 300 and 150 neurons respectively, are shown in Table. I. It can be clearly seen that if the size of the DNN is large enough (i.e., two hidden layers with 300 and 150 neurons respectively in this work), the recovery performance will not increase as the size of the DNN increases. Considering the memory effect of the RF-PA, the memory depth is set to 7. Since the training data and the true values are two complex-valued sets (I and Q), the number of neurons of the input layer and output layer is set to 14 and 2 respectively. In order to make the comparison fair, the memory depth of the MP-DSR technique is also set to 7. The DNN is trained using Python 3.7.0.

B. Computing resources analysis

The nonlinearity order of the MP model is set to 4. Then, the MP model used in the experiment can be represented as

$$r_{MP}[n] = \sum_{l=0}^{3} \sum_{m=0}^{6} a_{l,m} s[n-m] \, |s[n-m]|^{2l} . \quad (10)$$

Where a are the coefficients of the MP model. Then, it costs 189 real multiplications and 133 real additions.

Considering the number of neurons in each layer is 14, 300, 150, 2 respectively, there are at least 49500 real multiplications and 49964 real additions. However, the computing and power

resources are not an issue at ground stations as non-space level yet relatively low cost and significantly powerful computing resources, such as GPUs, are available. Therefore, although the DNN-DSR technique needs more computing resources than the MP-DSR technique, it would not limit the development of the deep learning technology in the space industry.

C. Relation between EVM, BER and SNR

The EVM is used to evaluate the performance of transmitters and receivers. In [27] and [28], the EVM-BER relation with different digital modulations is written as

$$\text{BER} = \frac{1 - M^{-1/2}}{0.5 \log_2 M} \text{erfc} \left[\sqrt{\frac{1.5}{(M-1)k^2 \text{EVM}_{\max}^2}} \right], \quad (11)$$

where $\text{EVM}_{\max}$ is measured when the maximum power of the ideal constellation vector is normalized to 1. The values of k^2 with different digital modulations are shown in Table. II.

Referring to (11), the EVM-BER relation is described in Fig. 10(a). As shown in the figure, when the EVM is lower than 10%, decreasing the EVM can dramatically improve the BER performance by several orders of magnitude. Then, from Fig. 10(b) that depicts different digital modulations with their theoretical BER curves, the EVM performance has a close connection with the output power of the transmitter.

D. Efficiency analysis

As mentioned in section I, there is a trade-off between the nonlinearity and power efficiency of the RF-PA. That trade-off can be clearly observed in Table. III, where the output of the RF-PA is analyzed in terms of the ACPR and EVM with different input powers of the RF-PA.

Fig. 11 specifies the measured recovery performance of the DNN-DSR and MP-DSR technique in terms of the EVM and ACPR, where the drain efficiency differences corresponding to the same distance on the abscissa are not equal. This is because the drain efficiency is measured after adjusting the output power of the signal generator with the same power step. The output power of the signal generator varies equidistantly; however, the drain efficiency varies not strictly equidistantly. Since the DSR technique is operated at the receiver side, we should pay more attention on the EVM rather than the ACPR to verify the DSR technique.

When the drain efficiency is about 45%, the DNN-DSR technique performs approximately 1% better than the MP-DSR technique in EVM. It is clearly observed in Fig. 10(a) that if the EVM is improved from 8% to 7% for the OFDM-16QAM modulation, the BER will drop from 1×10^{-5} to 8×10^{-7}. Consequently, we can change to a higher-order modulation to transmit more data using the DNN-DSR technique instead of the MP-DSR technique, while maintaining the same output power of the RF-PA.

More importantly, compared with the power back-off technique, the DNN-DSR technique can significantly improve the drain efficiency, while keeping the same EVM level. As depicted in Fig. 10(a), if the BER is required under 10^{-5}, the EVM will be restricted under 8% for the OFDM-16QAM

(a) Relation between the BER and EVM.

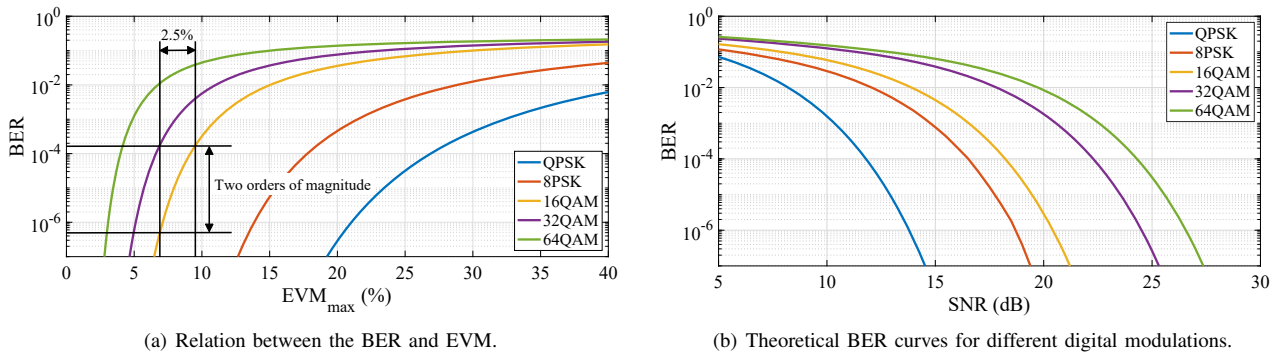(b) Theoretical BER curves for different digital modulations.

Fig. 10. Inter-dependencies between (a) BER and EVM, and (b) the theoretical BER curves for different digital modulations.

TABLE III
MEASURED EVM AND ACPR OF THE OUTPUT OF THE RF-PA WITHOUT USING ANY LINEARIZATION TECHNIQUES

Input power	33.85 dBm	33.35 dBm	32.85 dBm	32.5 dBm	32 dBm	30.95 dBm	30.05 dBm	29.45 dBm	28.95 dBm	28.5 dBm	27.6 dBm	26.45 dBm	26 dBm
Output power	38.6 dBm	38.4 dBm	38.15 dBm	37.9 dBm	37.7 dBm	37.3 dBm	36.7 dBm	36.45 dBm	36.15 dBm	35.75 dBm	35.1 dBm	34.35 dBm	33.98 dBm
Drain efficiency	46.2%	45.0%	43.6%	42.3%	41.7%	40.9%	38.3%	37.7%	36.6%	34.8%	32.6%	29.8%	28.4%
EVM	24.6%	23.0%	21.2%	19.5%	18.0%	14.8%	12.2%	11.1%	10.1%	9.4%	8.1%	7.4%	7.3%
ACPR	-20.9 dBc	-21.6 dBc	-22.4 dBc	-23.2 dBc	-24.0 dBc	-25.9 dBc	-27.8 dBc	-28.8 dBc	-29.8 dBc	-30.6 dBc	-32.1 dBc	-33.0 dBc	-33.3 dBc

(a) Measured relation between the drain efficiency and the EVM.

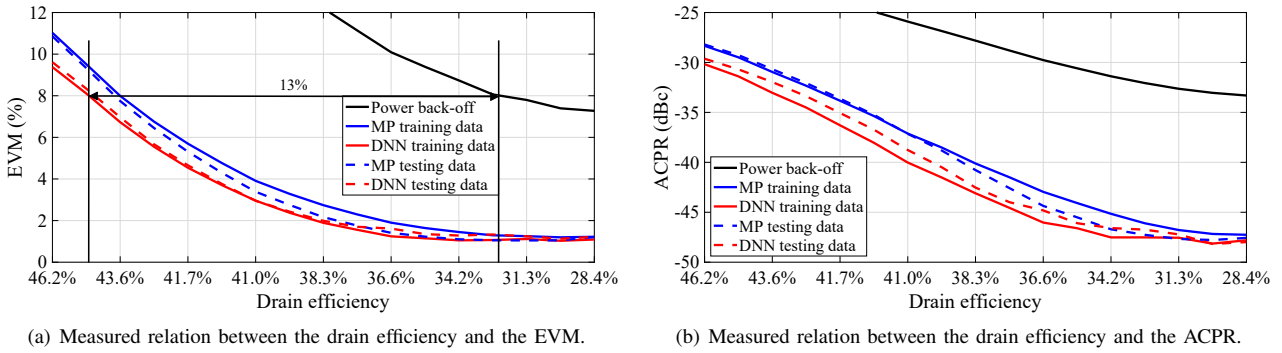(b) Measured relation between the drain efficiency and the ACPR.

Fig. 11. Measured recovery performance comparison of the DNN-DSR technique and the MP-DSR technique in terms of the ACPR and the EVM alone with the drain efficiency of the RF-PA. (a) Measured relation between the drain efficiency and the EVM, (b) Measured relation between the drain efficiency and the ACPR.

(a) EVM performance under the AWGN channel.

(b) ACPR performance under the AWGN channel.
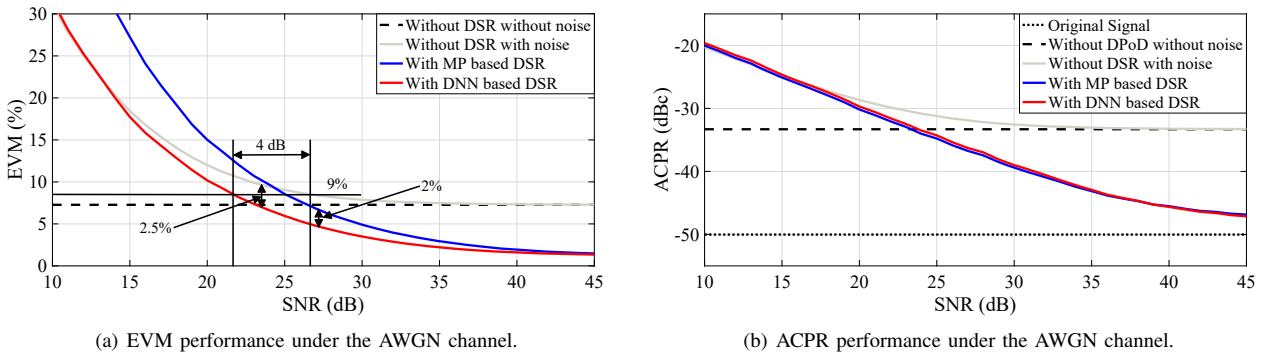
Fig. 12. Simulation results about the AWGN robustness comparison between the DNN-DSR technique and the MP-DSR technique in terms of the EVM and the ACPR. (a) EVM performance under the AWGN channel, (b) ACPR performance under the AWGN channel.

modulation. Fig. 11(a) specifies that the DNN-DSR technique can achieve almost 45% of the drain efficiency when an EVM of 8% is achieved, while the drain efficiency is only 32.6% by using power back off to obtain the same EVM level. In other words, the drain efficiency of the RF-PA can be increased from

32.6% to 45% using the DNN-DSR technique.

E. Noise robustness analysis

With a small input power of the RF-PA, it appears a slight nonlinearity, resulting in a low EVM level. It is clear to see

how the EVM changes under the AWGN channel. In this work, we utilize a small input power to analyze the recovery performance, which corresponds to the input power of 26 dBm in Table. III.

Fig. 12 describes the recovery performance of the two DSR techniques under the AWGN channel, in terms of the EVM and the ACPR. As can be seen, the recovery performance of the DNN-DSR technique is always better than that of the MP-DSR technique. Similarly, the ACPR is not important to qualify the performance of the DSR technique.

When the SNR is higher than 24 dB, the DNN-DSR technique outperforms the MP-DSR technique in SNR with 3 dB improvement under the same level of the EVM. In other words, the transmitted power can be reduced by up to 3 dB while maintaining the same EVM (i.e., the BER) by using the DNN-DSR technique instead of the MP-DSR technique. Particularly, when the SNR is 27 dB, the DNN-DSR technique can obtain approximately 2% improvement of the EVM, compared with the MP-DSR technique. Then, as shown in Fig. 10(a), above three orders of magnitude improvement of the BER can be achieved for the OFDM-32QAM modulation.

When the SNR is lower than 24 dB, the MP-DSR technique is not working at all. Compared with the communication system without using any linearization techniques (i.e., the gray line), if the EVM is required to be 9%, the DNN-DSR technique can achieve approximately 4 dB improvement of the SNR. Equivalently, the transmitted power can be reduced by 4 dB exploiting the DNN-DSR technique while maintaining the same BER. Furthermore, when the SNR is around 23 dB, above 2.5% improvement of the EVM can be obtained by using the DNN-DSR technique, compared with the communication system without linearization techniques. Then, for the OFDM signal with 16QAM modulation, from Fig. 10(a), about two orders of magnitude improvement of the BER can be obtained.

F. Power independence analysis

Since the input power of the RF-PA can affect the nonlinearity of the RF-PA, the input power should be kept constant in the power independence experiment. As an experiment, we also select a signal with a small input power but still contains sufficient nonlinear distortion, corresponding to the input power of 27.6 dBm in Table. III. Then, three groups of the output signals of the RF-PA, denoted as S_1, S_2, and S_3 respectively, are captured using different attenuators. The only difference between them is the power level, where the attenuation of the signal S_2 is regarded as 0 dB. Then, the attenuation coefficients of the signal S_1 and S_3 are relatively 6 dB and -6 dB, respectively, such that the signal power variation of the whole satellite communication window can be completely covered. To validate the power independence, signal S_2 is chosen to train the DNN and the MP model. The trained DNN and MP are both called M_2. Then, the signals S_1 and S_3 are used to finish the recovery.

Fig. 13 specifies the recovery performance comparison between the DNN-DSR technique and the MP-DSR technique with different signal powers, in terms of the power density

TABLE IV
MEASURED EVM AND ACPR OF THE OUTPUT OF THESE TWO DSR TECHNIQUES WITH THE DIFFERENT RECEIVED SIGNAL POWERS

DSR Model	M_2	M_2	M_2
Signal	S_1 (41.1 dBm)	S_2 (35.1 dBm)	S_3 (29.1 dBm)
EVM(DNN)	1.88%	1.86%	1.92%
EVM(MP)	1765.2%	1.61%	2.51%
ACPR(DNN)	-47.32 dBc	-46.71 dBc	-46.72 dBc
ACPR(MP)	-11.22 dBc	-47.48 dBc	-35.51 dBc

spectrum (PSD) and AM-AM curve. The gains, shown in Fig. 13(b) and Fig. 13(d), are measured with the effect of attenuators.

In contrast to the DNN-DSR technique, the MP-DSR technique is not working at all when the received signal power changes. Besides, it can be clearly observed in Fig.13(b) and Fig. 13(d) that the output power of the DNN always remains constant regardless of the change in the input power of the DNN. However, the output power of the MP-DSR technique varies with the input power.

The measured EVM and ACPR are given in Table. IV, where superior recovery performance of the DNN-DSR technique can be seen over the MP-DSR technique (Fig. 13(a)). The benefits of the DNN-DSR technique are further concluded as follows:

1) The DNN-DSR technique corrects the signal distortion caused by space-borne RF-PAs at the ground station, eliminating the need of DPD at the satellite, and hence saves space-borne computing resources.
2) The drain efficiency of the RF-PA can be increased to above 45% by using the DNN-DSR technique. Compared with the power back-off technique, the DNN-DSR technique can obtain up to 13% increase of the drain efficiency while maintaining the same EVM performance.
3) The MP-DSR technique cannot tolerate time-varying received signal power caused by time varying communication distances. However, this is not an issue for the DNN-DSR technique due to the BN layer.
4) The DNN-DSR technique is more robust to the AWGN than the MP-DSR technique.

VI. CONCLUSION

In this paper, we introduced a new DSR technique based on DNNs (DNN-DSR) for LEO satellite-to-ground communications. The DNN-DSR technique allows the space-borne RF-PA to work close to its saturation region, and hence has the ability to significantly increase the power efficiency of the satellites. The DNN-DSR technique features robustness against the noise and power variation, which makes it suitable to handle the additive white Gaussian noise (AWGN) channel and drastic power variation featured in LEO satellite-to-ground communications, while it is very challenging for conventional approaches. Seen from the experiment validation results, the DNN-DSR approach can increase the drain efficiency of a GaN RF-PA from 32.6% to 45% compared with the power back-off linearization technique. The results also show that the DNN-DSR approach relaxes the required transmitted power from the

(a) PSD of the output signal of the MP-DSR technique.

(b) AM-AM curve of the output signal of the MP-DSR technique.

(c) PSD of the output signal of the DNN-DSR technique.

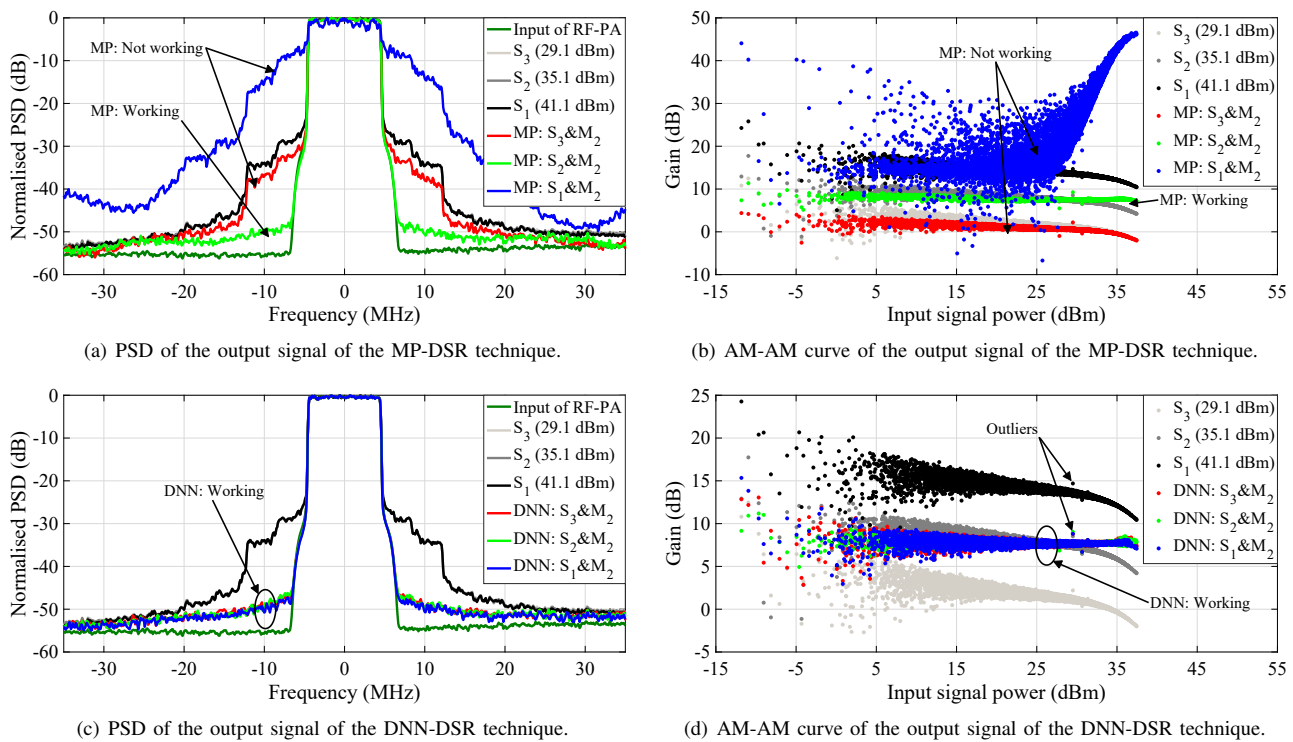(d) AM-AM curve of the output signal of the DNN-DSR technique.

Fig. 13. Measured PSD and the AM-AM for comparison of the DNN-DSR technique and the MP-DSR technique with the different received signal power. (a) PSD of the output signal of the MP-DSR technique, (b) AM-AM curve of the output signal of the MP-DSR technique, (c) PSD of the output signal of the DNN-DSR technique, (d) AM-AM curve of the output signal of the DNN-DSR technique.

satellite by up to 3 dB compared with the memory polynomial based digital signal recovery (MP-DSR). With such advantages and satisfactory performance, the DNN-DSR technique provides a promising solution to improve the transmission quality for LEO satellite-to-ground communication systems.

REFERENCES

[1] J. Wang, L. Li, and M. Zhou, "Topological dynamics characterization for LEO satellite networks," *Comput. Netw.*, vol. 51, no. 1, pp. 43–53, 2007.

[2] G. Araniti, I. Bisio, M. De Sanctis, A. Orsino, and J. Cosmas, "Multimedia content delivery for emerging 5G-satellite networks," *IEEE Trans. Broadcast.*, vol. 62, no. 1, pp. 10–23, Mar. 2016.

[3] A. Molina, K. Rajamani, and K. Azadet, "Digital predistortion using lookup tables with linear interpolation and extrapolation: Direct least squares coefficient adaptation," *IEEE Trans. Microw. Theory Tech.*, vol. 65, no. 3, pp. 980–987, Mar. 2017.

[4] D. R. Morgan, Z. Ma, J. Kim, M. G. Zierdt, and J. Pastalan, "A generalized memory polynomial model for digital predistortion of RF power amplifiers," *IEEE Trans. Signal Process.*, vol. 54, no. 10, pp. 3852–3860, Oct. 2006.

[5] Z. Su, J. Kolbusz, and B. M. Wilamowski, "Linearization of bipolar amplifiers based on neural-network training algorithm," *IEEE Trans. Ind. Electron.*, vol. 63, no. 6, pp. 3737–3744, Jun. 2016.

[6] R. G. Sáez and N. M. Marqués, "RF power amplifier linearization in professional mobile radio communications using artificial neural networks," *IEEE Trans. Ind. Electron.*, vol. 66, no. 4, pp. 3060–3070, Apr. 2019.

[7] L. D. Quach and S. P. Stapleton, "A postdistortion receiver for mobile communications," *IEEE Trans. Veh. Technol.*, vol. 42, no. 4, pp. 604–616, Nov. 1993.

[8] S. Yin, C. Liu, Z. Zhang, Y. Lin, D. Wang, J. Tejedor, T. F. Zheng, and Y. Li, "Noisy training for deep neural networks in speech recognition," *EURASIP J. Audio Speech Music Process.*, vol. 2015, no. 1, p. 2, Jan. 2015.

[9] K. Zhang, W. Zuo, Y. Chen, D. Meng, and L. Zhang, "Beyond a gaussian denoiser: Residual learning of deep CNN for image denoising," *IEEE Trans. Image Process.*, vol. 26, no. 7, pp. 3142–3155, Jul. 2017.

[10] M. Kim, W. Lee, and D. Cho, "A novel PAPR reduction scheme for OFDM system based on deep learning," *IEEE Commun. Lett.*, vol. 22, no. 3, pp. 510–513, Mar. 2018.

[11] T. O'Shea and J. Hoydis, "An introduction to deep learning for the physical layer," *IEEE Trans. Cogn. Commun. Netw.*, vol. 3, no. 4, pp. 563–575, Dec. 2017.

[12] N. Wu, X. Wang, B. Lin, and K. Zhang, "A CNN-based end-to-end learning framework toward intelligent communication systems," *IEEE Access*, vol. 7, pp. 110 197–110 204, 2019.

[13] J. Li, W. Xiong, G. Sun, Z. Wang, Y. Huang, and M. Shen, "Doppler-robust high-spectrum-efficiency VCM-OFDM scheme for low Earth orbit satellites broadband data transmission," *IET Commun.*, vol. 12, no. 1, pp. 35–43, Jan. 2018.

[14] I. Ali, N. Al-Dhahir, and J. E. Hershey, "Doppler characterization for LEO satellites," *IEEE Trans. Commun.*, vol. 46, no. 3, pp. 309–313, Mar. 1998.

[15] CCSDS 401.0-B-29, *Radio frequency and modulation systems - part 1 earth stations and spacecraft*, 2019.

[16] R. Zeng, H. Huang, L. Yang, and Z. Zhang, "Joint estimation of frequency offset and Doppler shift in high mobility environments based on orthogonal angle domain subspace projection," *IEEE Trans. Veh. Technol.*, vol. 67, no. 3, pp. 2254–2266, Mar. 2018.

[17] P. W. Kinman, S. M. Hinedi, R. C. LaBelle, R. P. Bevan, H. M. Del Castillo, and D. C. Chong, "Digital Doppler measurement with spacecraft," *IEEE Trans. Instrum. Meas.*, vol. 40, no. 4, pp. 727–731, Aug. 1991.

[18] S. Ioffe and C. Szegedy, "Batch normalization: Accelerating deep network training by reducing internal covariate shift," *arXiv preprint arXiv:1502.03167*, 2015.

[19] X. Glorot, A. Bordes, and Y. Bengio, "Deep sparse rectifier neural networks," in *Proc. Int. Conf. AI Statistics*, vol. 15, pp. 315–323. PMLR, Apr. 2011.

[20] R. Girshick, "Fast R-CNN," in *Proc. IEEE Int. Conf. Comput. Vision*, Dec. 2015.

[21] D. P. Kingma and J. Ba, "Adam: A method for stochastic optimization," *arXiv preprint arXiv:1412.6980*, 2014.

[22] ROHDE&SCHWARZ, *R&S SMBV100A vector signal generator specifications*, Jul. 2018.

[23] ROHDE&SCHWARZ, *R&S FSQ signal analyzer specifications*, Jun. 2011.

[24] CREE, *CGH40006, 6 W, GaN HEMT by cree for general purpose (CGH40006P) (wireless devices) transistor*, May. 2015.

[25] OPHIRRF, *Model 5303125, 0.7–4.0 GHz, 6 w, Linear power RF amplifier*, Jun. 2013.

[26] Inmarsat, "Strategic review of satellite and space science use of spectrum," Inmarsat, Tech. Rep., Jun.-Aug. 2015.

[27] H. A. Mahmoud and H. Arslan, "Error vector magnitude to SNR conversion for nondata-aided receivers," *IEEE Trans. Wireless Commun.*, vol. 8, no. 5, pp. 2694–2704, May. 2009.

[28] R. Schmogrow, B. Nebendahl, M. Winter, A. Josten, D. Hillerkuss, S. Koenig, J. Meyer, M. Dreschmann, M. Huebner, C. Koos, J. Becker, W. Freude, and J. Leuthold, "Error vector magnitude as a performance measure for advanced modulation formats," *IEEE Photon. Technol. Lett.*, vol. 24, no. 1, pp. 61–63, Jan. 2012.

Yufeng Zhang was born in Altay, China. He received the B.Eng. degree in electronic engineering from University of Electronic Science and Technology of China (UESTC) of Chengdu, China in 2015. He is currently working towards the Ph.D. degree in electromagnetic field and microwave technology at the University of Chinese Academy of Sciences (UCAS), Beijing, China. He is currently a guest Ph.D. student with the Department of Electronic Systems at Aalborg University, Aalborg, Denmark.

His research interests include artificial neural networks and its application for communication systems.

Zhugang Wang was born in Hangzhou, China. He received the B.Sc degree in information and electronics from Zhejiang University of Zhejiang, China in 1995. He obtained the M.Sc. degree in engineering from the Department of Computer Science at Tsinghua University of Beijing, China in 2003. In 2017, He achieved his Ph.D. degree in satellite communication engineering from University of Chinese Academy of Sciences (UCAS) of Beijing, China.

He is currently a researcher at National Space Science Center of Chinese Academy of Sciences in Beijing, China. Over the past decade, he has hosted or participated in several satellite TT&C communication projects. His current research interests include communications, ranging, and synchronization in satellite constellations.

Yonghui Hunag was born in Anshan, China. He received the B.Sc. degree in electronics engineering from Tsinghua University of Beijing, China in 1998. In 2001, he obtained the M.Sc. degree in aero-spacecraft design from University Chinese Academy of Sciences of Beijing, China. He achieved the Ph.D. degree in wireless communication from Aalborg University of Aalborg, Denmark in 2008. He is currently a professor with National Space Science Center of Chinese Academy of Science in Beijing, China. From 2002 to 2011, He worked as a Postdoc. and research assistant in Aalborg University of Aalborg, Denmark.

He was a engineer in Datang Mobile of Beijing, China from 2001 to 2002. His current research interests include deep space communication, satellite wireless communication, phased array antenna, transmitter linearization. He is the TPC member of IEEE CCET and IEEE WiSEE.

Wei Wei was born in Shanxi, China. He received the bachelor degree in information engineering from Communication University of China in 2001. In 2009, he obtained the master degree in microwave and photonics engineering from Chalmers University of Technology, Sweden. In 2014, he achieved the Ph.D degree in wireless communication from Aalborg University, Denmark.

He has more than 10 years of experiences in antenna and RF design from several MHz to milimeter-wave frequency. His favourite topics include power amplifiers, waveguide devices and phased array antennas. He currently works for Danfysik A/S as an RF expert.

Gert Frølund Pedersen (M'14) was born in 1965. He received the B.Sc. and E.E. (Hons.) degrees in electrical engineering from the College of Technology in Dublin, Dublin Institute of Technology, Dublin, Ireland, in 1991, and the M.Sc.E.E. and Ph.D. degrees from Aalborg University, Aalborg, Denmark, in 1993 and 2003, respectively. Since 1993, he has been with Aalborg University where he is a Full Professor heading the Antennas, Propagation and Millimeter-wave Systems LAB with 25 researchers. He is also the Head of the Doctoral School on wireless communication with some 40 Ph.D. students enrolled. His research interests include radio communication for mobile terminals especially small antennas, diversity systems, propagation, and biological effects. He has published more than 500 peer reviewed papers, 6 books, 12 book chapters and holds over 50 patents. He has also worked as a Consultant for developments of more than 100 antennas for mobile terminals including the first internal antenna for mobile phones in 1994 with lowest SAR, first internal triple-band antenna in 1998 with low SAR and high TRP and TIS, and lately various multiantenna systems rated as the most efficient on the market.

He has worked most of the time with joint university and industry projects and have received more than 21 M$ in direct research funding. He is currently the Project Leader of the RANGE project with a total budget of over 8 M$ investigating high performance centimetre/millimeter-wave antennas for 5G mobile phones. He has been one of the pioneers in establishing over-the-air measurement systems. The measurement technique is now well established for mobile terminals with single antennas and he was chairing the various COST groups with liaison to 3GPP and CTIA for over-the-air test of MIMO terminals. He is currently involved in MIMO OTA measurement.

Ming Shen (M'11) was born in Yuxi, China. He received the M.Sc. degree in electrical engineering from University of Chinese Academy of Sciences (UCAS), Beijing, China in 2005. In 2010, he obtained his Ph.D. degree in Wireless Communications, with the Spar Nord Annual Best Thesis nomination, from Aalborg University, Denmark. He is currently an associate professor in RF and mm-wave circuits and systems with the Department of Electronic Systems, Aalborg University, Denmark. He has 20 years experience in RF and millimeter wave circuits and systems, including 12 years experience in CMOS RF/mixed-signal IC design. His current research interests include circuits and antennas for 5G and satellite communications, low power CMOS RF and millimeter wave circuits and systems, circuits and systems for biomedical imaging, and artificial intelligence.

Dr. Shen is the grant holder and PI of two Danish national research projects, and the management committee member substitute from Denmark in the EU COST Action IC1301 with the aim to gather the international efforts and address efficient wireless power transmission technologies. He is a member of IEEE, the TPC member of IEEE NORCAS, serves as a reviewer for IEEE and Kluwer.